THESIS FOR THE DEGREE OF LICENTIATE OF ENGINEERING

Characterization of injection molded polymers
– from conventional to wood-based thermoplastics

Linnea Björn

Department of Physics

CHALMERS UNIVERSITY OF TECHNOLOGY

Gothenburg, Sweden 2022

Characterization of injection molded polymers – from conventional to wood-based thermoplastics
Linnea Björn

Department of Physics
Chalmers University of Technology
SE-412 96 Gothenburg
Sweden
Telephone + 46 (0)761264758

Cover: Multilayer morphology of injection molded polyethylene measured with scanning SAXS

Printed by Chalmers Reproservice
Gothenburg, Sweden 2022

Characterization of injection molded polymers
– from conventional to wood-based thermoplastics

Linnea Björn
Department of Physics
Chalmers University of Technology

Abstract

The success of polymers products is associated with the melt processability, which allows to create products with complex shapes at a low cost. One of the most widely used processing techniques utilizing melt processability is injection molding, where a polymer is heated until it flows into a mold under pressure. Due to varying shear- and cooling rates during processing, injection molding creates a multilayered structure, consisting of complex hierarchical morphologies. In addition to process conditions, the structures formed are dependent on the molecular architecture including chemical environment and branching of the polymer chain. The resulting morphology defines the mechanical properties of the injection molded parts and consequently, understanding the correlation between material, processing parameters, and resulting morphology is an important challenge. Furthermore, to expand the use of injection molding to renewable cellulosic materials, intrinsic limitation in cellulose that impede melt processing must be overcome. This can be achieved by chemically modifying the cellulose, however chemical modifications impact the morphology formed during processing.

This thesis focuses on using advanced scanning small- and wide-angle X-ray scattering as main characterization techniques, to unfold the nature of the complex semicrystalline structures in injection molded synthetic and cellulose-based polymers. By varying material parameters, processing conditions and using complementary techniques, such as computational simulations and mechanical testing, the underlying factors for formation of hierarchical morphologies is further studied. This thesis brings us one step closer to understanding and predicting the polymer microstructures and resulting mechanical properties of injection molded materials.

Keywords: Hierarchical Materials, Polyethylene, Dialcohol cellulose, melt processing, injection molding, SAXS, WAXS

List of Papers

This thesis is based on the following papers:

I Scanning Small-angle X-ray Scattering of Injection Molded Polymers: Anisotropic Structure and Mechanical Properties of Low Density Polyethylene

Linnea Björn, Renan Melhado Mazza, Eskil Andreasson, Fredrik Ottenklev, Viviane Lutz Bueno, Manuel Guizar Sicairos, Elin Persson Jutemar and Marianne Liebi

In manuscript

II Process induced structures of Injection Molded High Density Polyethylene – combining X-ray Scattering and Finite Element Modeling

Linnea Björn, Elin Persson Jutemar, Renan Melhado Mazza, Eskil Andreasson, Fredrik Ottenklev, Manuel Guizar Sicairos, and Marianne Liebi

In manuscript

III Melt processed materials of exceptionally high cellulose fibre content

Giada Lo Re, Emile R. Engel, Linnea Björn Manuel Guizar Sicairos, Marianne Liebi, Jan Wahlberg, Katarina Jonasson, Per A. Larsson

Submitted to Nature 11 May 2022

Contribution Report

I L.B planned and performed the experimental work together with M.L, V.L.B and M.G.S for the X-ray experiments and E.P.J for the mechanical testing. E.P.J performed DSC experiments and R.M.M performed the computational simulations. L.B analyzed the scattering data and prepared the manuscript, where E.P.J and R.M.M prepared parts of DSC and Computational Simulations. All authors discussed the results and reviewed the manuscript.

II L.B planned and performed the experimental work together with M.L, and M.G.S for the X-ray experiments. L.B performed birefringence measurements, F.O performed Light Optical measurements and R.M.M performed the computational simulations. L.B analyzed the scattering data and prepared the manuscript, where E.P.J and R.M.M prepared parts of DSC and Computational Simulations. L.B and E.P.J prepared the draft, where all authors discussed the results and reviewed the manuscript.

III L.B, and M.L performed WAXS measurements with the assistance of M.G.S, analysed and wrote of the corresponding paragraphs.. G.L.R did conceptualization, methodology, validation, formal analysis, investigation, data curation, writing, review and editing, supervision and funding acquisition. E.R.E did data curation, writing, review and editing. J.W and K.J performed pilot scale melt processing of the bottle caps and permeability tests, P.A.L did conceptualization, writing and review.

Abbreviations

DAC – Dialcohol cellulose
DSC – Differential scanning calorimetry
EAA – Ethylene acrylic acid
FEM – Finite element method
HDPE – High density polyethylene
LDPE – Low density polyethylene
LOM – Light optical microscopy
LV LDPE – low viscosity low density polyethylene
MFI – melt flow index
MV LDPE - medium viscosity low density polyethylene
SAXS – Small angle X-ray scattering
STXM – Scanning transmission X-ray microscopy
V/P – Volume/Pressure
WAXS – wide angle X-ray scattering
XRF – X-ray fluorescence

Table of Contents

Chapter 1

Introduction

From the toothbrush we use in the morning to the fabrics in our clothes, polymer materials are present in all aspects of our daily life. During the past centenary the use of plastics has exponentially increased, to the point that today it is hard to imagine modern day society without man-made polymers. The rapid growth of plastic use can to a large extent be explained by extraordinary material properties, high processability and low price. The beginning of the polymer age can be traced back to the 1950s where large-scale production of plastic started and since then, production rates have increased yearly by an average annual growth rate of 8.2%, up to 2020 when the Covid 19 pandemic impacted the industry (Figure 1.1).

The largest market for plastic material is packaging[2], where the leading factor for the rapid growth was a global shift from reusable to single use containers. The most common polymer for packaging is polyethylene[3], and globally a total of 90 million metric tons of polyethylene is annually produced[4]. In many commercial applications, the mechanical performance of the

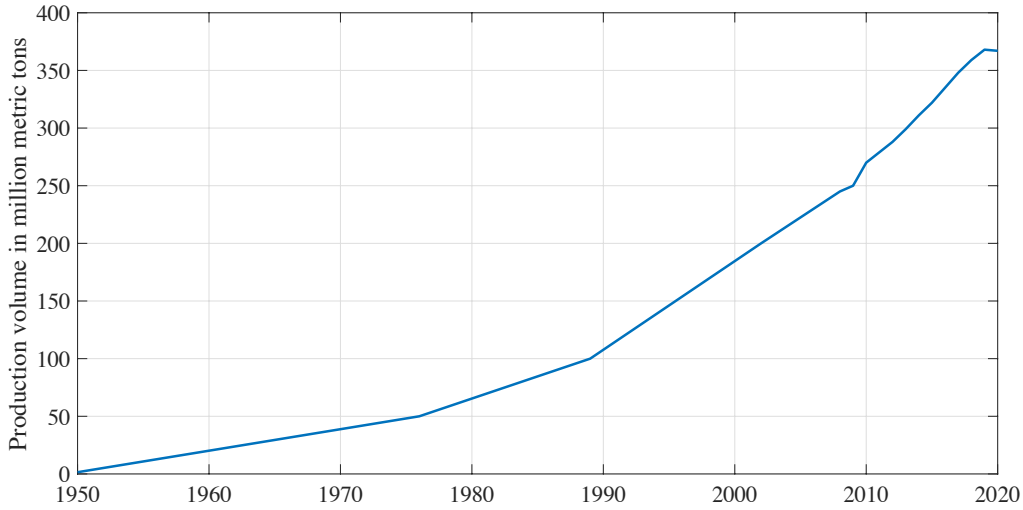

Figure 1.1 Annual production of plastic from 1950-2020 in million metric tons. Source: Statista[1]

material is of high importance to ensure the quality of the product, where ductility, strength and fracture behaviour of the polymer is of particularly high interest.

The micro- and nanostructures of a polymer material are highly influenced by the processing, and in-depth understanding of the structure-processing relationship is a prerequisite to tailor material properties of plastic products. To correlate molecular structures with the mechanical properties of the material, several aspects such as degree of crystallinity and structural orientations must be taken into consideration. Furthermore, material factors including molecular weight, polymer branching, and additives influence the molecular structure formed. Due to the complexity of the system and the number of factors that impacts the results, many of the underlying relations are still not clear.

The vast majority of plastics are derived from fossil-based hydrocarbons and thereby these materials do not naturally degrade. The plastic waste annually created must either be eliminated by combustion which results in greenhouse emissions or being put on landfill. An estimation made by Geyer et al.[2] is that daunting 12,000 Mt of plastic waste will end up in landfill by 2050 if current production and waste management continues. A response to this is an increasing interest for bio-degradable materials from sustainable resources that can replace the fossil-based plastics. Cellulose is a promising candidate since it is one of the most abundant biopolymer on earth[5]. It is furthermore degradable and can easily be processed into a two-dimensional material such as paper or board[6]. However, conventional processing methods of polymer materials such as injection molding requires the material to have thermoplastic properties. That is, the material should become soft and amendable for molding upon heating or shearing and become rigid and retain the molded shape upon cooling. Cellulose fibres are intrinsically not thermoplastic and thereby can not be melt processed into complex three-dimensional shapes without first chemical modification of the cellulose.

In this thesis, hierarchical structures from the Angstrom regime to the millimeter scale of injection molded synthetic and wood-based polymers have been investigated by using scanning small- and wide-angle x-ray scattering in combination with complementary techniques. The starting point was to study commercially used polyethylene with varying densities, molecular weights, and process conditions to shed light on the relationship between structure, processing, and mechanical performance. The experimental data was further compared with computational simulations to explore the underlying mechanisms for the anisotropic morphologies. In the future, these results could be used to calibrate simulation models, which could be used to predict material performance without the need for physical tests of each prototype with varying complex shapes and materials. This will enable prompt implementation and optimization of new sustainable polymer materials. As a next step, a novel cellulose-based composite was studied, where scanning wide angle x-ray scattering was used to investigate how degree of modification and material composition induce structural changes throughout the material. Understanding how hierarchical structures change throughout polymer material is key to optimize material usage, further increase the quality of the product and to develop more sustainable materials.

Chapter 2

Polymers

A polymer is a large molecule that forms long chains made up by covalently bonded repeating units. The most common state for molecular order in these long chains is crystalline where long enough polymer chains fold back on themselves and form crystalline lamellae[7], with the direction of the polymer chain perpendicular to the direction of the lamellae. However, due to kinetic effects and intrinsic disorder built into the polymer chains, the crystallisation process is most often not complete, resulting in a semicrystalline structure with amorphous regions in between the crystallites[8].

From a thermodynamic process, in order for crystallisation of a polymer to take place, the Gibbs free energy, G, must be negative

$$G = H - TS \qquad Equation\ 2.1$$

where H is enthalpy, S is entropy and T is temperature. The crystallisation process is associated with a large negative entropy change since the molecular order of the polymer chains increases. Thereby, for Gibbs free energy to be negative, there must be a matching negative enthalpy change, which implies that strong interactions between polymer chains are necessary for crystallisation to take place. Linear polymer chains allow for the polymers to pack closely, which increases the interaction between the chains. Thus, linear polymers are more prone to form crystals, compared to branched polymers with many defects incorporated into the polymer chain.

The folded surface is associated with large interfacial energy, which would thermodynamically favour thick lamellae crystals. However, due to kinetic limitations, polymers are found to form lamellae with a thickness typically in the range of tens of nanometers. The larger number of folds increase the free energy but make crystallization more kinetically accessible[9]. The thickness of the crystalline lamellae is highly dependent on the temperature of the melt at which the crystallization takes place[10] .

Individual polymer chains may be involved in several crystalline lamellae as well as the amorphous regions in between[11]. In a similar way, the crystalline lamellae often consist of multiple polymer chains, as an entangled configuration retains the maximal entropy resulting in a complex intertwined network structure[12]. The length of the polymer chains and the number of entanglements makes the crystallisation process a complex and kinetically controlled process[13].

If polymer crystallisation takes place in a melt under quiescent conditions, crystallites tend to grow in a random fashion resulting in a state with low degree of molecular orientation, whereas if the polymer chains are subjected to either a shear or an elongational flow, alignment of the molecular chains can be achieved[14]. The ordered arrangement of crystalline polymers imparts high strength and rigidity, with a direction dependent response due to the predominant crystal alignment[15], where the process induced differences in microstructure can provide orders of magnitude variation in physical properties of a given polymer[16].

2.2 Polyethylene

From a chemical point of view, polyethylene is one of the simplest polymers since it consists of repeating units of methylene. However, from a structural point of view the structure is often quite complex. The most common crystalline state of polyethylene is packing of unbranched parts of the polymer chains into an orthorhombic unit cell, with amorphous regions in-between the crystalline parts[17, 18]. If crystallisation occurs in a melt at rest, the lamellae of polyethylene grows around central nucleolus resulting in a isotropic crystal structure called spherulites[19]. If crystallisation instead takes place at intermediate shear, the spherulites elongate in the direction of the flow, adapting to more or less elliptical shapes[16, 20]. At high shear, a so called shish-kebab morphology can be formed where polymer chains are stretched out in the direction of the flow creating highly oriented thread-like structures (shish) with crystalline lamellae (kebabs) grown in the perpendicular direction[21, 22]. Figure 2.1 shows schematic representations as well as microscopy images of the spherulite and shish-kebab microstructure. The spherulite structure is associated with isotropic mechanical properties[23], whereas the Shish-kebab structure gives highly anisotropic properties where the tensile strength is improved and the elongation at break is decreased in the direction of the oriented shish[24, 25]. The Shish-kebab structure is more prone to form when the cooling rates are high[26], and it has been reported to have two different morphologies with twisted and untwisted lamellae[22, 27].

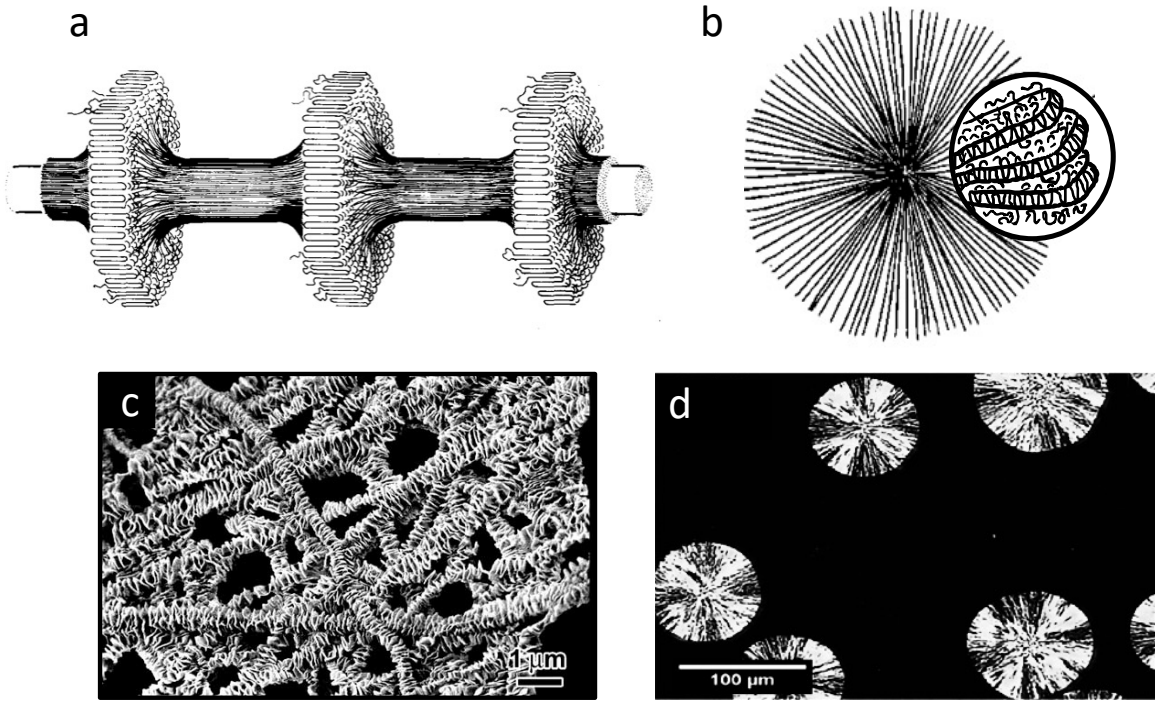

Figure 2.1 Examples of semicrystalline morphologies of polyethylene. Figure 2a and 2b show schematic representation of the shish-kebab and spherulite microstructure respectively, Figure 2c shows micrographs of the shish kebab structure taken with field-emission scanning emission microscopy, and Figure 2d shows polarized optical microscopy images of a spherulite microstructure. Adapted with permission from Katti et al[16] (Copyright 2004, John Wiley & Sons), Somani et al.[28] (Copyright 2005, Elsevier) and Tong et al.[29] (Copyright 2015, Elsevier).

2.3 Cellulose

Cellulose can be derived from numerous sources for example wood, agricultural waste[30], and oil palm biomass residue[31], making it an abundant material. The structure of native lignocellulose is highly hierarchical and complex, as shown in Figure 2.2, where the sizes and

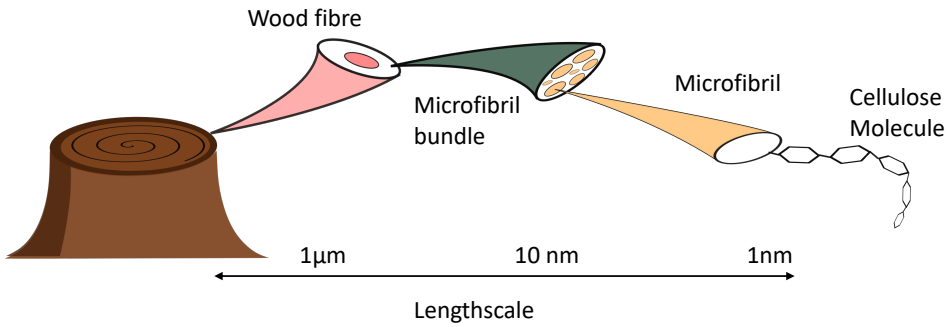

Figure 2.2 The hierarchical structures of wood. Inspiration from Penttilä[32]

distribution of the components can differ depending on the plant species and environmental influences[33].

Cellulose is a linear polymer composed of glucose[34] and the molecular structure of cellulose can be seen in Figure 2.3a (i). In similarity to other polymers, cellulose is a semicrystalline material forming both amorphous and crystalline regions, where the cellulose chains stack together with intramolecular hydrogen and van-der-Waals bonds to form the crystalline regions. The assembly of cellulose chains form nano-sized structures called microfibrils, which has an approximate diameter of 2-20 nm and an approximate length of 0.1-40 μm[35]. The fibrils exhibit high strength and are therefore considered to be reinforcement components of the wood fibers[36]. The microfibrils further aggregate to microfibril bundles which are parts of the wood fibers.

Cellulose is not intrinsically thermoplastic and in order to use it in conventional processing techniques like injection molding, modification of the cellulose structure is needed. A promising cellulose modification is dialcohol cellulose (Figure 2.3a), since this material has been shown to exhibit thermoplastic properties in terms of softening, increased ductility, and melt processability[37]. The suggested structure for the heterogeneously modified dialcohol cellulose is a core-shell structure, with amorphous dialcohol cellulose as a shell around a core of more crystalline cellulose as shown in Figure 2.3b. One hypothesis is that thermoplastic properties are achieved from a combination of surface modification enhancing the fibre-fibre interphase, and internal modification making the fibre more flexible.

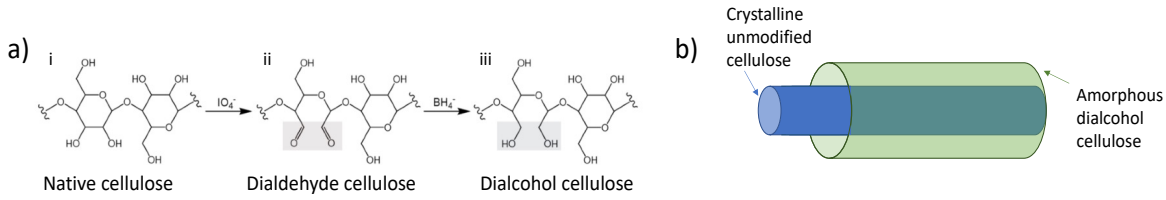

Figure 2.3 Structure of dialcohol cellulose where a) shows the reaction scheme and b) shows schematic representation of the fibril structure of diacohol cellulose. The core consists of crystalline cellulose and the surface consists of amorhous dialcohol cellulose.

Chapter 3

Injection Molding

Injection molding is a widely used processing technique for polymers that has been developed for almost 150 years[38] and over 30% of all plastic parts are manufactured with injection molding[39]. In the injection molding process, plastic pellets are fed into the injection molding machine and heated until the polymer is soft enough to be injected into a mold under pressure. This creates a complex flow pattern called fountain flow (Figure 3.1) with varying shear and cooling rates in the through-thickness direction, highly influencing the hierarchical semicrystalline structure of the polymer. Several studies have been published investigating how various processing conditions influence the polymer morphologies, such as pressure[40, 41], shear rate[42] cooling rate[43] and stress overshoot[44]. Kattis et al[16] described that close to the injection molded gate the flow has a semicircular shape mainly dominated by an elongational flow, whereas further down the plate the flow is laminar instead. Thus, it is expected that the polymer morphology depends both on the position in the thickness direction as well as the distance from the injection molded gate.

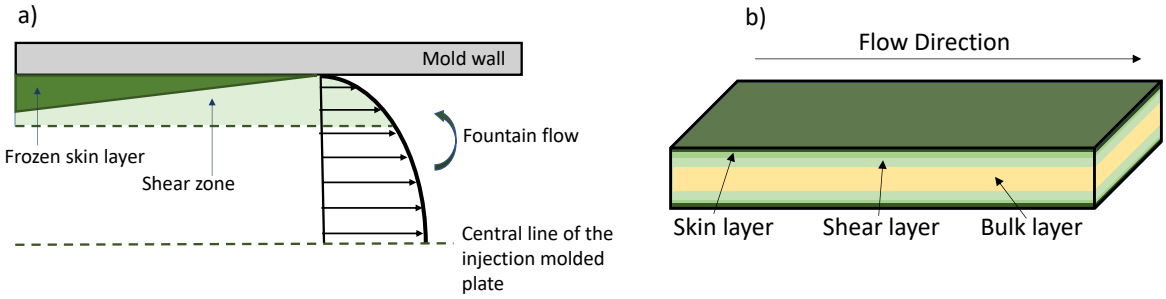

Figure 3.1 Multilayered structure of injection molded polymers, where a) shows the shear rate profile of the fountain flow inspired by Zhou et al.[45], and b) shows the characteristic layers of an injection molded plate.

The injection molded process can be divided into four stages[46]. First is the filling phase where the molten polymer is injected into the cool mold under pressure. Second is the packing phase, where high pressure is maintained and additional melt flows into the cavity to prevent shrinkage under solidification. Third comes the cooling phase where the polymer is allowed to cool down to room temperature and last is the ejection, where the polymer is removed from the injection molding machine. A schematic representation of volume flow rate, pressure, temperature, and crystallization progress can be seen in Figure 3.2.

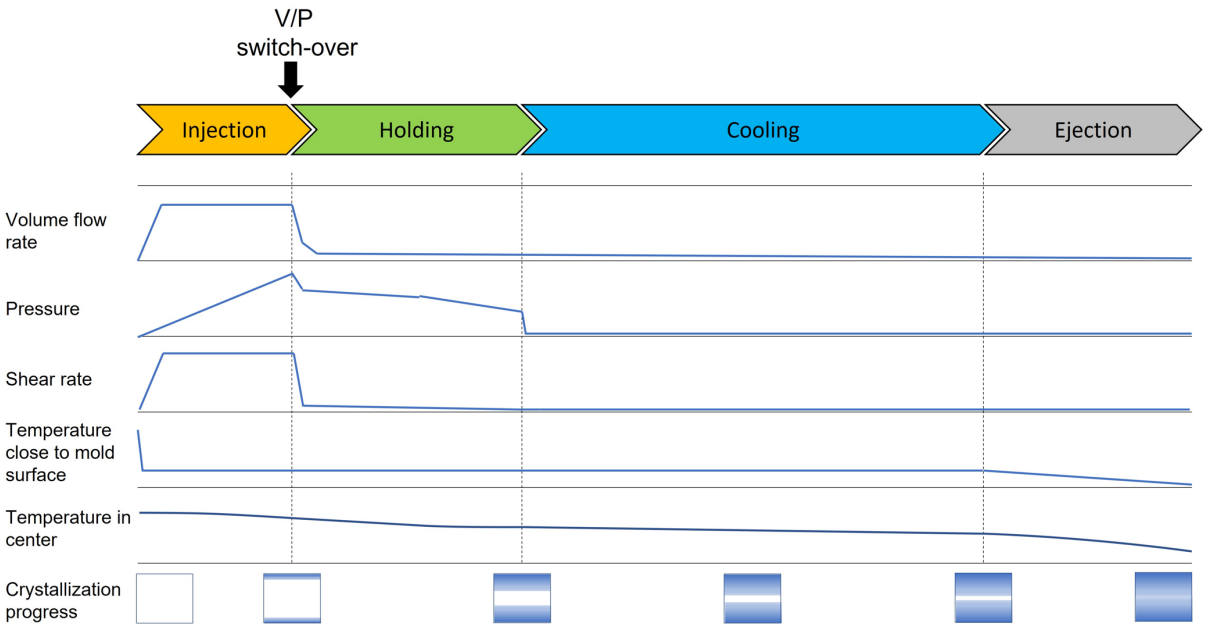

Figure 3.2 Schematic representation of the different phases during injection molding. The figure is taken from paper II.

Chapter 4

Materials and Experimental Methods

4.1 Materials and Sample Preparation

In this thesis two types of materials have been studied, on the one hand polyethylene with varying densities, and viscosities and on the other hand mixtures of dialcohol cellulose (DAC) and Ethylene Acrylic Acid Copolymer (EAA).

Both high-density polyethylene (HDPE) and low-density polyethylene (LDPE) were used, with two types of LDPEs with varying viscosity and one type of HDPE. The LDPEs had a density of 923 kg/m^3 and the HDPE had a density of 953 kg/m^3. The Melt Flow Index (MFI) was 55 g/10 min for the low viscosity LDPE, 22 g/10 min for the medium viscosity LDPE and 26 g/10 min for the HDPE min when measured at 190 ºC at a load of 2.16 kg.

The DAC was derived from bleached softwood kraft fibres by using oxidation and reduction with sodium periodate and sodium borohydride respectively, according to a partly modified version of an earlier described protocol[37, 47]. This resulted in conversion of cellulose to dialcohol cellulose with varying degrees of modification. The cellulose was then mixed in with EAA to create cellulose composites.

The sample for scanning SAXS, WAXS and birefringence were prepared by cutting slices of 50 μm using a Microtome (Leica RM2255 from Triolab for LDPE and HDPE and RMC MT-XL ultramicrotome for cellulose-based samples). LDPE and HDPE were evaluated in two separate directions, CD-TD and MD-TD as described in Figure 4.1.

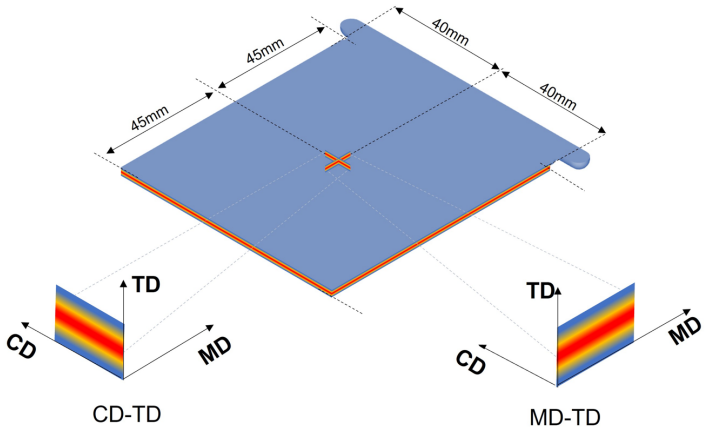

Figure 4.1 Injection-molded test plate with dimensions and positions of the measured samples. The layered structure along the thickness direction (TD) was studied by preparing cross-section in CD-TD, and MD-TD plane, respectively. The figure is taken from Paper II

4.2 Small and Wide angle X-ray scattering

X-ray scattering is a non-invasive technique sensitive to structural changes on Angstrom to nanometer range, where the signal is the average of all structural components over the whole depth of the illuminated sample volume. A typical experimental set up is shown in Figure 4.2, where a monochromatic X-ray beam with wave vector $\overrightarrow{k_i}$ is focused on a sample in transmission mode. Parts of the radiation will be scattered at an angle 2θ as defined by the vector $\overrightarrow{k_s}$ where the scattering intensity is measured by the detector behind the sample. The scattering pattern recorded is the square of the Fourier transform of the electron-density distribution with the sample[48]. Constructive interference is achieved when Braggs law is fulfilled,

$$n\lambda = 2dsin(\theta) \qquad \text{Equation 4.1}$$

where n is a positive integer, λ is the wavelength of the X-rays, d is the distance between the repeating structure and θ is the scattering angle. In case of repeating units in the material, Braggs law will be fulfilled, and a peak appears in the scattering data. When analysing a scattering pattern, it is convenient to define a scattering vector $\vec{q}$ as

$$\vec{q} = \overrightarrow{k_i} - \overrightarrow{k_s} \qquad \text{Equation 4.2}$$

In case of elastic scattering, the scattering vector $\vec{q}$ fulfills Braggs law and can thus be described as

$$|\vec{q}| = q = \frac{4\pi}{\lambda} sin\theta \qquad \text{Equation 4.3}$$

By substituting for $\frac{\sin(\theta)}{\lambda}$ in equation 4.1 a simple relationship between the scattering vector $\vec{q}$ and repeating distance d is obtained, which is independent on the energy of the X-ray beam.

$$q = \frac{2\,\pi}{d} \qquad \text{Equation 4.4}$$

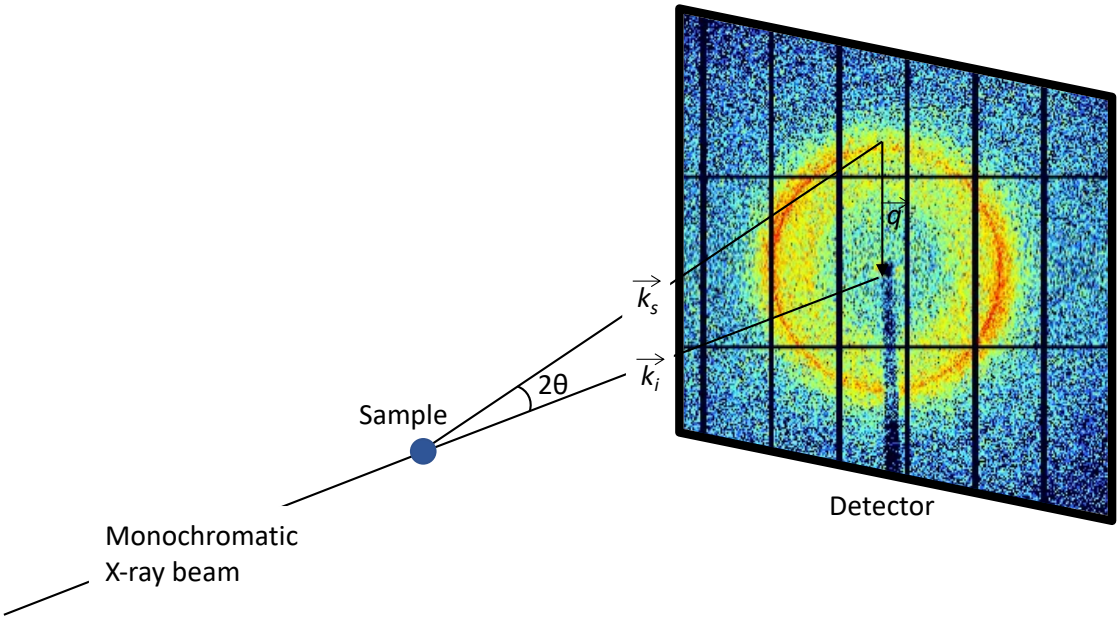

Figure 4.2. Transmission setup of the scattering experiment.

Since the repeating distance d is inversely proportional to both the scattering vector q and the scattering angle θ, structures of different sizes can be investigated by resolving either the small- or the wide angles of the X-ray scattering. In practice this is done by changing the sample to detector distance. In Small Angle X-ray Scattering (SAXS) the detector is typically placed meters away from the sample, which provides information on relatively large repeating structures inside the material, generally in the range of a few nanometers to hundreds of nanometers. In synthetic polymer materials, the SAXS signal is commonly used to characterize lamellar spacing[49] whereas in cellulose-based materials the SAXS signal can be used to investigate distances between the fibrils[50]. In WAXS the detector is placed centimeters away from the sample instead, providing information on small repeating structures in the Angstrom regime. In the crystalline regions of polymer materials, the positions of the atoms are well defined giving rise to sharp WAXS peaks corresponding to the distance between atom planes. In addition, amorphous regions exhibit short-range order due to chemical van der Waals forces between polymer chains, giving rise to a broad WAXS-peak[51, 52].

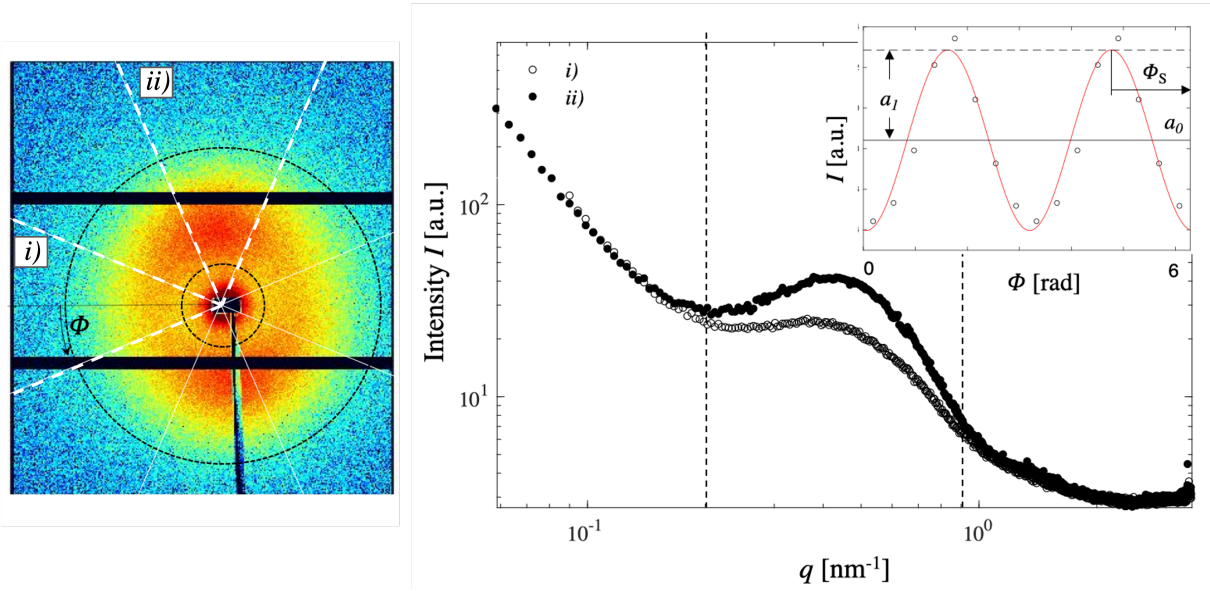

Figure 4.3. SAXS 2D pattern (left) and integrated intensity (right) of the skin layer of medium viscosity LDPE. The radial integration is performed in a horizontal i) and vertical azimuthal segment ii). The inset shows the azimuthal integrated intensity capturing the asymmetry of the scattering pattern in the q-range from 0.26 - 0.94 nm^{-1} as indicated with dashed circles and dashed lines, respectively. The figure is taken from Paper I.

The scattering data was analysed according to the approach proposed by Bunk et al.[53] where each 2D scattering pattern is dived into to N_θ azimuthal segments, in this work N_θ= 16 segments were used. The azimuthal intensity distribution is approximated over the segments with a cosine function, as shown in the inset in Figure 4.3, where the measured values are indicated with black circles and the cosine approximation is shown in red. The baseline of the cosine function a_0 gives the symmetric intensity, which correspond to the average scattering of the sample whereas the amplitude of the cosine function a_1 gives the asymmetric intensity which corresponds to the oriented part of the scattering. The degree of orientation can be defined as the ratio a_1/a_0 and the phase of the signal Φ_s corresponds to the angle of orientation.

4.3 Scanning SAXS and WAXS

All scattering experiments presented in this thesis were performed at the cSAXS beamline X12SA at the Paul Scherrer Institute (PSI, Switzerland) using scanning SAXS/WAXS, i.e. the samples were scanned through the X-ray beam and a scattering pattern was collected for each position of the scan. The micro-focused beam in combination with the high flux made it possible to investigate structural changes throughout extended areas of the samples, making scanning SAXS and WAXS suitable methods to investigate hierarchical structures, from the angstrom regime to the millimeter scale.

A Si(111) double crystal monochromator was used to select the X-ray energy of 11.2 keV for LDPE samples and 12.4 keV for HDPE and cellulose-based samples where the beam size varied between 4*42 μm to 40 x 40μm. A Pilatus 2M detector[54] was used to record the scattering signal where the distance between the samples and detector was 25 cm for WAXS-setup and varied between 2.1669-2.171m for the SAXS-setup. When measuring in SAXS, a flight tube of 2 m was placed in between the sample and the detector to reduce air scattering and X-ray absorption. The exposure time used was 0.1 s for LDPE samples and 0.06s for HDPE- and cellulose-based samples.

4.4 Mechanical Testing

In commercial application, the inherent toughness and resistance to fracturing of a polymer material is of outermost importance. Since polyethylene is a widely used polymer material, the mechanical response of polyethylene has been extensively studied with most studies focusing on isotropic polyethylene[55-59], and with a few studies published on anisotropic polyethylene with flow induced structures[60,61]. Mechanical testing is also a common approach to characterize cellulose-based polymers. However, since cellulose is known to be a highly heterogenous material with structural variation depending on raw material[62], growing conditions of the plant[63], potential thermal treatments[64], and chemical modifications[65], the mechanical behaviour highly varies between different studies.

One of the most widely used approaches to study mechanical characteristics of polymer materials is to measure the stress-strain behaviour, where a tensile force is applied to the sample and the resulting deformation of the sample is measured. This gives information on the modulus, brittleness, and strength of the polymer. An example of a stress-strain curve can be seen in Figure 4.4, showing the elastic and plastic regions. In the elastic region, the polymer can go back to its original shape if the tensile force is removed. At a certain threshold called the yield point, the polymer reaches its elastic limit and beyond this point the deformation of the polymer is permanent. This is called the plastic region, and here the elongation of the sample will continue at almost constant stress until the ultimate elongation is reached and the polymer breaks. A polymer is defined as brittle if the polymer fractures before the yield point is reached, whereas the polymer is defined as ductile if the polymer elongates in to the plastic region[49].

In this thesis, during the characterization of the polyethylene materials a standard tensile test equipment Zwick Z010 Proline [ZwickRoell, Germany] was used with a load cell of 1 kN. The tests with a loading rate of 100 mm/min and a gauge length between the grips of 58 mm. 10 samples were measured for each material, and the results were averaged to obtain the stress-strain curve.

The characterization of the cellulose-based materials was performed by Giada Lo Re using a single column Instron 5944 (Norwood, Massachusetts, USA) tensile micro tester with a load

cell of 2 kN. The tests were performed with a loading rate of 15 mm/min using a gauge length between the grips of 30 mm. Five samples were measured for each material composition.

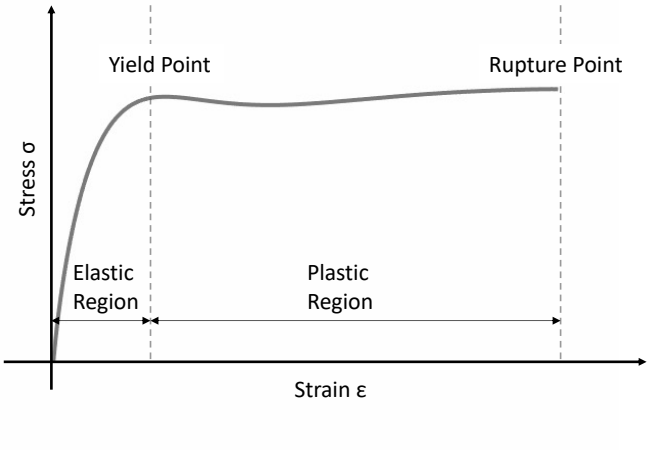

Figure 4.4 Stress-strain response of a typical polymer.

4.5 Birefringence Microscopy

Birefringence is an optical property of a material where the refractive index is dependent on the polarization and propagation direction of the light. When a birefringent material is exposed to light, the incident ray of light is split into two rays with opposite polarisations. The two rays are called the ordinary ray and the extraordinary ray, where the ordinary ray propagates through the material with the same velocity in every direction, whereas the velocity of the extraordinary ray is dependent upon the propagation direction within the crystal. The Birefringence B is defined as

$$B = |n_e - n_o|$$

where n_e is the refractive index of the extraordinary ray and n_o is the refractive index of the ordinary ray. To relate the velocity difference between the ordinary and extraordinary rays as they propagate through the sample, the retardation Γ can be used

$$\Gamma = t * B$$

where t is the thickness of the sample.

Birefringence in polymer material is a consequence of optical anisotropy which is affected by molecular orientation of the polymer chains[66]. In this thesis, the retardance and angle of the optical fast axis was measured with a birefringence imaging microscope (EXICOR MICROIMAGERTM, Hinds Instruments, Inc., OR) to investigate the multi-layered structure of injection molded HDPE. The setup used consisted of a linear polarizer at 0°, a photo-elastic

modulator (PEM) at 45°, a PEM at 0° and a liner polarizer at 45°. Due to the high level of birefringence, phase unwrapping technology included in the Hinds software was used, which combined measurements from four stroboscopic light sources (LED, with wavelength 655nm, 615nm, 530 nm and 475 nm). The samples were measured with a 10x objective in front of a 2048*2048 pixel 12-bit CCD camera resulting in a spatial resolution of 0.5μm/pixel and a field of view of 1 mm*1 mm.

Chapter 5

Results

This thesis aims to study the hierarchical structures formed during injection molding of synthetic and wood-based polymers. The main focus was using advanced scanning SAXS and WAXS since these methods provide in-depth information on the structures present, as well as achieve high spatial resolution. In addition, several complementary techniques were used with the aim of understanding the conditions needed for certain structures to form as well as their impact on the mechanical performance of the injection molded parts.

5.1 Using scanning SAXS and WAXS to study a flow induced multi-layered morphology

Scanning X-ray scattering techniques were used to evaluate the structures of injection molded synthetic and wood based polymers. A multi-layered morphology could be observed in all samples investigated, where the degree of orientation was highest close to the edge of the sample as shown in Figure 5.1. Detailed descriptions of the layered morphology of LDPE can be found in Paper I, of HDPE in Paper II and of cellulose composite in Paper III. The multi-layered structure is a consequence of the injection molding process, where high shear close to the edge inflict orientation of the polymer chains and fast cooling from the cold mold freezes the structures in place. The different materials were prepared with different process settings, making it difficult to compare absolute values of the degree of orientation, both between polyethylene and cellulose, as well as between HDPE and LDPE. Furthermore, the different materials are composed of different hierarchical structures, where the degree of orientation is highly affected by the form of the structures. For example, perfectly aligned thin fibres will give higher degree of orientation values compared to perfectly aligned ellipsoids with low aspect ratio between the axis, particularly in the SAXS regime.

Figure 5.1a-d shows degree of orientation values of the diffraction peak for SAXS of LDPE and HDPE respectively, for two perpendicular directions (MD-TD and CD-TD according to Figure 4.1), where the diffraction peak corresponds to the center-to-center distance of the crystalline lamellae. Note that different q-regions were used to evaluate the degree of orientation, where a q-region of 0.26 - 0.94 nm^{-1} was used for the LDPE, whereas a q-region

of 0.145-0.623 nm^{-1} was used for the HDPE. The q-region was adapted for the different materials since increased density of polyethylene is associated with increased lamellae thickness[67]. In the LDPE, four distinct layers could be identified (Figure 5.1a-b), where the two outer layers mainly were distinguishable in the CD-TD direction. The HDPE showed a more complex structure with more pronounced difference in the layered distribution between the two measuring directions (Figure 5.1c-d), compared to LDPE. By combining data from both SAXS and WAXS (Figure 5.1c-e), five distinct layers could be identified for HDPE. The more complex morphology in HDPE compared to LDPE is believed to be a consequence of less branching of the chain, making HDPE more prone to form highly ordered crystalline structures.

Comparing the degree of orientation in WAXS between HDPE and the cellulose-based composite, HDPE gives rise to significantly higher degree of orientation values and sharper transitions between the different layers (Figure 5.1e-f). This is hypothesized to be a result of the well defined hierarchical structures polyethylene can form. Above a certain threshold values of shear- cooling rate and pressure, polyethylene is transitioned from a spherulite to a shish-kebab microstructure causing a drastic change of the scattering signal, as discussed in detail in Paper II. Cellulose on the other hand cannot form such structures due to more intrinsic disorder built into the polymer chains, resulting in less long range order and an overall lower degree of orientation. Crystalline parts of cellulose, have been reported to consist of roughly 15-30 cellulose chains which corresponds to crystalline regions of 2-4 nm[68-70]. This is considerably smaller than the crystalline regions of polyethylene, where typical sizes of the crystalline lamellae are around 10 nm thick and 1-50 um long[71, 72].

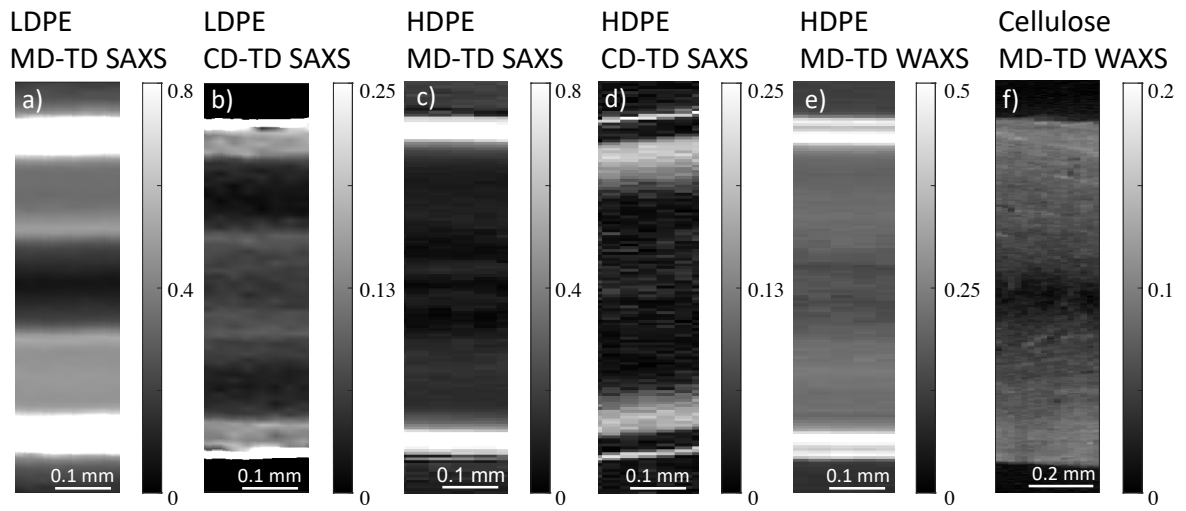

Figure 5.1. Degree of Orientation calculated for a-b) SAXS long distance peak of LDPE c-d) SAXS long distance peak of HDPE, e) WAXS (110)-peak of HDPE and f) WAXS (110)-peak of cellulose in a EAA polymer matrix. The SAXS results are taken from two perpendicular planes, MD-TD and CD-TD respectively.

By combining 2D scattering patterns from both SAXS and WAXS, more in-depth information of the hierarchical structures can be revealed. Figure 5.2, shows four examples of 2D scattering patterns of HDPE, where the scattering patterns in a) were collected from the edge of the plate, and in b) a bit further into the bulk of the plate. Exact measuring points of the scattering patterns in Figure 5.2 as well as more examples of 2D scattering patterns throughout the sample can be seen in Figure 3 in Paper II and S3 and Supplementary information of Paper II. The SAXS 2D data in a) show a weak tendency for a vertical streak and a two-point pattern in the horizontal direction. This scattering pattern indicates the presence of a shish-kebab crystalline structure, where the streak represents the shish and the two-point patterns represent the aligned lamellae in the kebabs. WAXS 2D pattern has four maxima scattered as a cross along the horizontal plane in the (110) crystal plane, two maxima along the vertical plane in the (200) crystal plane, and two broad maxima along the horizontal plane in the (020) crystal plane. This is a typical WAXS scattering pattern for shish-kebab with twisted lamellae, as indicated by the schematic to the right[22,73]. In b) the vertical streak in the SAXS signal is less pronounced, whereas the two point pattern are more intense, indicating less shish-structures present in the sample and more growth of the crystalline lamellae. In WAXS, the crystal (110)-, (200)-, and (020)-planes are aligned in the vertical direction. These are typical characteristics for shish-kebab with untwisted/regular lamellae. In order to reveal the type of shish-kebab structure present, a combination of SAXS and WAXS 2D patterns must be used.

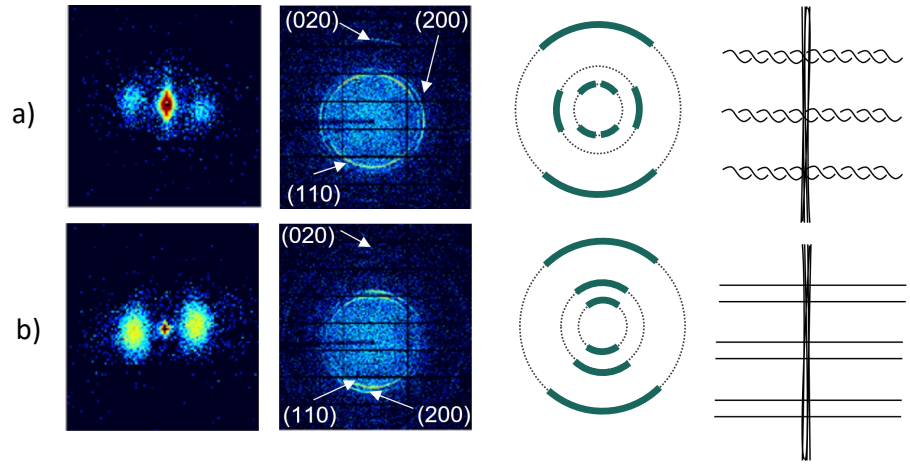

Figure 5.2 Examples of 2D SAXS and WAXS scattering patterns, clarification of the WAXS pattern as well as a schematic of the structure indicated by the scattering patterns. Row a) correspond to a position at the edge of the sample close to the mold whereas row b) correspond to a position further into the sample.

To further evaluate and compare how choice of material, distance to injection gate and process settings impacts the multi-layered morphology, the scattering signal of scanning SAXS and WAXS was evaluated throughout the thickness of injection molded plates (Figure 5.3). By utilizing the highly focused beam and high flux provided at the synchrotron, small differences of the layered morphology could be evaluated.

In the LDPE, the focus was evaluating differences of varying viscosities of the polymer, and in position of the plate. Figure 5.3a shows that medium viscosity LDPE on average exhibit a higher degree of orientation than low viscosity LDPE. It was also seen that the distance between the injection gate and the measuring point had high impact on the structures formed, where a higher degree of orientation was found closest to the inlet of the mold (position 1). By using computational simulations (Figure 6 and 7 in Paper I), it was found that the origin of the more oriented structures in medium viscosity LDPE compared to low viscosity LDPE is a higher shear rate in combination with a higher cooling rate during processing, whereas the difference seen in scattering data from different positions of the plate could be explained by having longer time under shear as well as higher shear rate in position 1.

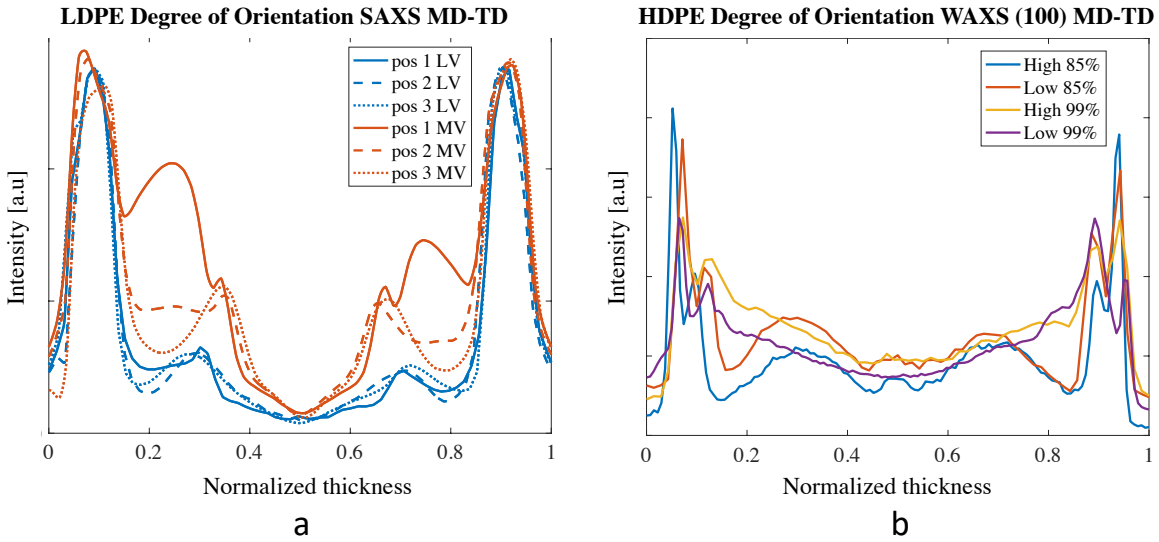

Figure 5.3. Degree of orientation calculated along a line through the thickness of a) SAXS of LDPEs with varying viscosities and positions of the injection molded plate and b) HDPEs produces with different process settings.

HDPEs were used to evaluate the influence of different processing settings, where both difference in injection speed (high and low) and difference in the volume/pressure (V/P) switchover point was varied. The V/P switchover point is defined as the transition between the injection- and packing phase according to Figure , and in this study we investigate samples where the switchover point occurred at either 85% or 99% filing of the cavity volume. Figure 5.3b shows that the V/P switchover point has a more significant influence on the layered morphology than the injection speed, in particular in the highly oriented layers close to the injection mold. By using computational simulations (Figure 9 in Paper II), we could conclude that the difference in orientation is most likely a consequence of the higher pressure used during the holding phase for the 85% samples.

To investigate how the morphology of LDPE was changed upon deformation and fracture, deformed samples after tensile testing were measured post-mortem with scanning SAXS (Figure 5.4) both in top-view where the average structure through all layers were measured (Figure 5.4a) and with side view where the structure of each layer were evaluated separately (Figure 5.4b). The colours in the Figure 5.4 correspond to the preferred scattering direction

where blue colour indicates horizontally aligned scattering and red indicates vertically aligned scattering. From the top view sample, a clear necking region could be identified where the main scattering direction changed from blue in undeformed regions to red in deformed regions, indicating a change from preferred orientation of the long axis in the direction of the flow, to preferred orientation in the direction of the applied stress occurred. Thus, the macroscopic deformation is reflected in the underlying nanostructure. The side view samples (Figure 5.4b), show the layered morphology through the thickness before and after deformation. It can be seen that the orientation of the skin layer close to the edge is intact also after deformation, whereas the shear and bulk layers change the orientation deformation direction. These observations agree well with the results published by Guo et al[74] where crystalline segments, formed by slip of lamellae, beyond the yield point reorient into the direction of the deformation. More measurements of deformed samples including peak fitting can be seen in Figure 9 and 10 in Paper I.

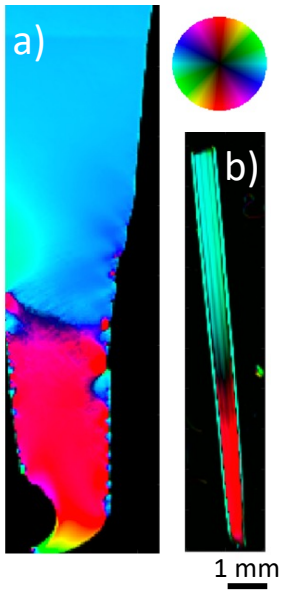

Figure 5.4 Scanning SAXS of a medium viscosity LDPE dogbone deformed in CD direction for top view (a) and side view(b).

The cellulose-based materials investigated are two component systems consisting of modified cellulose and EAA-polymer matrix. Figure 5.5a shows radially integrated WAXS data from different compositions of fibre and cellulose, where the top curve in light blue corresponds to 100% modified cellulose fibres, and the bottom dark blue curve corresponds to 100% EAA. Some parts of the cellulose and EAA spectra have little overlap, for instance in the region of q=10.2-10.7 nm^{-1} corresponding to the cellulose (110)-peak and q=24.8-25.9 corresponding to the EAA (020)-peak. Thereby, orientation effects of cellulose and EAA could be evaluated separately, as shown in Figure 5.5b-c. The degree of orientation of the cellulose (Figure 5.5b) shows a soft gradient from the edge to the center of the sample, whereas in the EAA polymer (Figure 5.5c), similar to the polyethylene samples, sharp transitions between different layers where observed. This information is useful for understanding how threshold values of pressure, shear and temperature affects different types of material. The 2D scattering pattern

from three different positions in the samples in Figure 5.5 show that the preferred direction of the scattering is mainly in the vertical directions close to the edge, which indicates that the polymer chains are oriented in the direction of the flow, whereas almost no preferred scattering direction can be observed in the center of the sample.

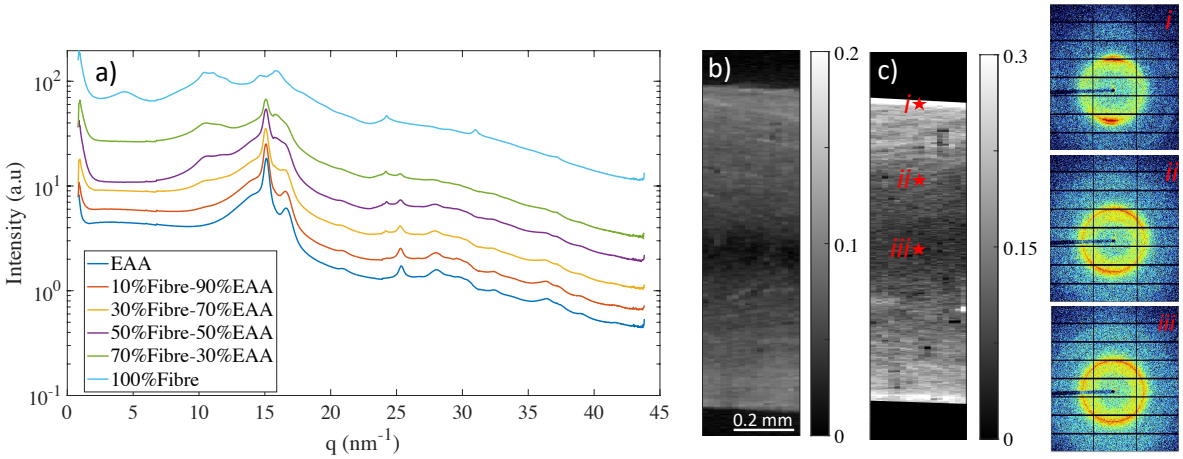

Figure 5.5 WAXS results from cellulose-based composites where a) shows integrated scattering intensity for EAA, fibre composites and modified cellulose, b) shows degree of orientation calculated for the cellulose (110)- peak and c) shows degree of orientation calculated for the EAA (020)-peak for a composite that consists of 70% cellulose fibres and 30% EAA. In addition, some selected 2D scattering patterns are showed for three positions in c).

5.2 Combining scattering data with complementary methods

In the thesis, emphasis was put on how scanning SAXS and WAXS can be combined with complementary techniques to further understand the hierarchical structures of injection molded polymers. A summary with a few selected examples will be described in the section below, where more examples can be found in Paper I, Paper II and Paper III including mechanical testing (Paper I and Paper III), birefringence measurements (Paper II), light optical microscopy (Paper II), DSC (Paper I and III) and computational simulations (Paper I and II).

Tensile testing was used to correlate the morphology to mechanical performance of the material. Stress-strain curves from the different viscosities of LDPE is shown in Figure 5.6, where orange curves correspond to low viscosity LDPE, blue curves correspond to medium viscosity LDPE and dots and crosses indicate the break points for the 10 samples measured. Both low- and medium viscosity LDPE showed a higher ultimate strength in the MD direction compared to the CD direction. The difference between material strength in MD compared to in CD could be explained by the orientation of the highly oriented shish-kebab microstructure in the skin layer, as well the oriented elongated spherulite microstructure which were

identified using scanning SAXS (Figure 3 Paper I). The shish-kebab structure has been reported to improve the tensile strength in the direction of the fibril-like shish [25, 75, 76], explaining the higher ultimate strength measured in MD. When comparing low and medium viscosity LDPE using scanning SAXS (Figure 4 Paper I), it was concluded that medium viscosity LDPE had thicker skin layers, as well as more oriented and thicker shear layers compared to low viscosity LDPE. The higher tensile strength and higher stiffness observed in medium viscosity LDPE compared to low viscosity LDPE can be explained by the difference in thickness of highly oriented layers.

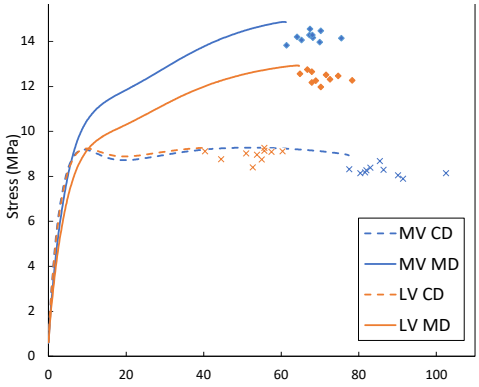

Figure 5.6 Stress Strain curves of LDPEs with low (LV)- and medium viscosity (MV).

Birefringence microscopy was used for HDPE samples produced with different process settings to further evaluate how process condition influence the layered morphology. Figure 5.7 shows the result, where the colour indicates the direction of the angle of the fast axis. Similar to the SAXS results (Figure 5.3b and Figure 8 in Paper II), it was found that samples produced with the 85% V/P point had a significantly different layered structure with the presence of the thick layer of highly oriented crystalline morphology oriented vertically as indicated by the red colour. Overall, a good agreement was found between SAXS and Birefringence results. Correlating scattering results with birefringence is of importance in an industrial point of view since birefringence microscopy is more available and requires less data analysis compared to scanning SAXS and WAXS. Furthermore, birefringence measurements provide higher spatial resolution, allowing resolution of finer layers. However, the birefringence measurements by themselves do not provide enough information to define the hierarchical structures present, making the two techniques complementary to each other.

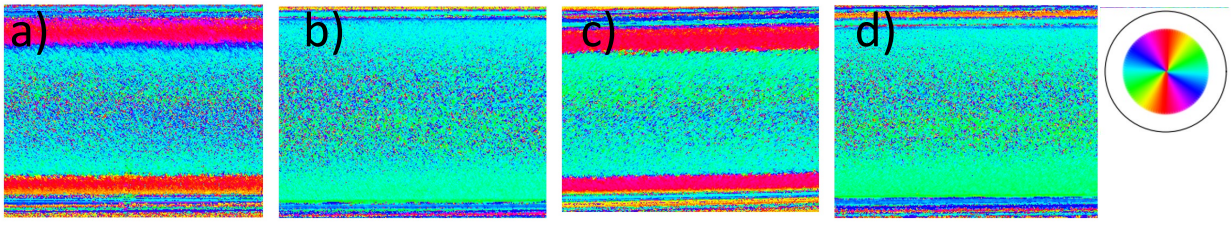

Figure 5.7 The angle of fast axis measured with birefringence microscopy for a) HDPE High 85%, b) HDPE High 99%, c) HDPE Low 85%, and d) HDPE Low 99%.

Chapter 6

Conclusions and Outlook

The work presented in this thesis shows that advanced scanning SAXS and WAXS are powerful techniques to investigate hierarchical flow induced structures in polyethylene and cellulose-based composites, in particular when the scattering data is combined with other techniques such as tensile testing, birefringence microscopy and computational simulations. All samples studied showed a clear multi-layered morphology as a consequence of varying shear-, temperature- and pressure-profiles during processing. For the LDPE samples, the work was centered around understanding the link between processing, morphology, and mechanical performance (Paper I). Scanning SAXS was used to gain insight on hierachical structures of the different layers, computational simulations were used to evaluate the shear- and temperature profiles in the through-thickness direction, and tensile testing was used to show the mechanical performance of LDPEs with different viscosities at varying distances from the injection gate. The combination of scattering data, simulations and mechanical testing revealed that oriented shish-kebab and elongated spherulite microstructures contribute to high tensile strength when deformed in the direction of the flow. Moreover, it was shown that the molecular weight of the polymer and the position on the injection molded plate highly influenced the hierarchical structure formed, where higher degree of orientation was found in higher molecular weight samples close to the injection flood gate. By measuring scanning SAXS on deformed samples post mortem the deformation mechanisms could be further studied. It could be concluded that when samples are deformed perpendicularly to the flow, the orientation of the highly oriented shish-kebab structures close to the mold wall stays intact upon deformation whereas layers consisting of elongated spherulites and randomly oriented spherulites changes its orientation in the direction of the applied stress.

An interesting aspect for future studies would be to investigate the deformation process of polymer materials using SAXS and WAXS *in-situ*, that is to repeatedly collect scattering patterns for one point in the sample while deforming it. This would provide important insights how the microstructures are changed while being deformed, which could further reveal the link between hierarchical morphologies and the mechanical performance. Previous studies of polyethylene have reported a stress-induced martensitic transformation of the unit cell, in which the orthorhombic structure of undeformed polyethylene is converted to a monoclinic structure[77, 78], however this is not something that can be observed by measuring deformed samples post mortem.

HDPE chains are less branched compared to LDPE and are therefore more prone to form crystalline structures. Consequently, a more complex layered morphology was expected in the HDPE samples compared to the LDPE samples. In the work presented, a combination of scanning SAXS, WAXS, birefringence and light optical microscopy was used to get a more in-depth understanding of the layered morphology of HDPE, which resulted in identification of more distinct layers compared to LDPE. HDPE samples produced with different process settings were characterized to further evaluate how process conditions influence the hierarchical structures, and it was found that the pressure during the holding phase of injection molding had a higher influence on the molecular structures than the injection speed.

The work on cellulose-based composites was centered around use of scanning WAXS to visualize distribution and orientation of cellulose within a EAA polymer matrix. Since there was little overlap between the cellulose (110)- peak and the EAA (020)- peak in WAXS, these peaks were used to separately evaluate orientation effects of the polymer and the cellulose. A homogenous distribution of cellulose was found within all samples measured, indicating a good mixing between the cellulose and EAA. Furthermore, a loss in degree of orientation was found for cellulose with higher degree of modification whereas the degree of orientation of the EAA was unaffected with the degree of orientation of the cellulose.

One of the most severe short-comings with dialcohol cellulose is that it is difficult to process dry material, resulting in high process forces and high temperatures causing discoloration of the material. This can be overcome by addition of water during the processing, making it possible to process dialcohol cellulose at temperatures below 140°C. Thereby, another interesting aspect for future studies would be to use scanning WAXS and SAXS to investigate how the hierarchical structure within dialcohol cellulose is affected by added water during processing. So far, our work has been focused on the WAXS signal of cellulose-based materials, however previous studies have showed that in systems where microfibrils are packed with high regularity, a peak in SAXS appears corresponding to the mean center-to-center microfibril spacing [50,79] . The SAXS signal could thereby be used to investigate if water aided processing gives swelling effects on fibrils, which we hypothesize can be correlated with the thermoplastic properties of the material. A combination of SAXS and WAXS would thereby give a more complete understanding of the hierarchical structures in dialcohol cellulose.

In addition, it would be of high interest to use SAXS and WAXS to investigate structural changes of modified cellulose while the material is being heated, that is continuously collecting scattering patterns while the temperature of the sample is increased. Understanding such structural changes in-situ would provide useful information on how the material is affected by increased temperatures, which is key for understanding the conditions needed to achieve thermoplastic properties of cellulose materials.

Furthermore, we plan to use other types of X-ray-based synchrotron methods to characterize cellulose-based materials, such as scanning transmission X-ray microscopy (STXM) based on the near edge X-ray absorption spectral (NEXAFS) contrast and X-ray fluorescence (XRF). In STXM, the X-ray transmission can be measured as a function of the energy of the X-ray beam. If the X-ray energy is varied over the absorption edge of carbon, different chemical bonds that includes carbon atoms can be detected, making it possible to map out chemical modifications commonly used in cellulose. The STXM-method provide a high spatial resolution below 50 nm[80], and could thereby be used to determine where in the samples chemical modifications are situated. If the chemical modifications contain elements not intrinsically present in the cellulose, scanning X-ray fluorescence could be used in a similar way, with the aim to receiving chemical maps of the chemical modifications. Furthermore, XRF can be measured together with SAXS and WAXS, making it possible to investigate both structural and elemental changes simultaneously [81, 82].

Acknowledgements

First, I would like to thank the Swedish Innovation Agency VINNOVA and the competence center FibRe for providing funding for this work. I also thank the EUSMI program and the Paul Scherrer Institute for granting access to synchrotron radiation beamtime at the cSAXS beamline at Swiss Light Source.

Marianne, I am incredibly grateful for you giving me the opportunity of doing a PhD, for everything you taught me and for your patience with me. Thank you for giving me the freedom to explore my own ideas and for believing that I can do this, even when I doubt it myself.

A huge thank you to the people I have worked with at Tetra Pak. Elin, Renan, Eskil, Fredrik and Daniela. For all your enthusiasm and for the countless hours of scientific discussions, without you this work would not have been possible.

Thank you, Giada, for teaching me about cellulose-based materials, I hope we will do more collaborations in the future. Thank you, Aleksandar, for always providing help whenever I needed it and for creating a great atmosphere at the division and thank you Anette for always being excited when we discuss about science.

The biggest thanks go to all my colleagues at the Material Physics division, you make ordinary days so much more fun. A special thanks to my office mates, Adrian and Filippa for being by my side since my first day of the PhD and to Linnea R, for the great experience working with you during the spring.

I would also like to thank the extended Liebi group, even if we are physically in different locations, you make it feel like we are close by. Thank you for all for all the input to my work and for the great times we had during the group workshops.

Finally, the biggest thanks go to my friends and family, thank you for all the love and support. Thank you, John, for always being there for me and for bringing me up whenever things get hard.

Bibliography

1. Tiseo, I. Global plastic production 1950-2020. https://www.statista.com/statistics/282732/global-production-of-plastics-since-1950/.

2. Geyer, R.; Jambeck, J.; Law, K., Production, use, and fate of all plastics ever made. *Science Advances* 2017

3. PlasticsEurope Plastics-the Facts 2021. https://plasticseurope.org/wp-content/uploads/2021/12/Plastics-the-Facts-2021-web-final.pdf.

4. Demirors, M., The History of Polyethylene. In 100+ Years of Plastics. Leo Baekeland and Beyond, *American Chemical Society:* **2011**

5. Ganie, S. A.; Ali, A.; Mir, T. A.; Li, Q., 5 - Fabrication and characterization of cellulose-based green materials. *Advanced Green Materials,* Ahmed, S., Ed. Woodhead **2021**

6. Moon, R.; Martini, A.; Nairn, J.; Simonsen, J.; Youngblood, J., ChemInform Abstract: Cellulose Nanomaterials Review: Structure, Properties and Nanocomposites. *Chemical Society reviews* **2011**

7. Keller, A.; Mackley, M., Chain orientation and crystallization. *Pure and Applied Chemistry - PURE APPL CHEM* **1974**

8. Strobl, G., *The Physics of Polymers. Concepts for Understanding Their Structures and Behavior*. **2007**.

9. Verho, T.; Paajanen, A.; Vaari, J.; Laukkanen, A., Crystal Growth in Polyethylene by Molecular Dynamics: The Crystal Edge and Lamellar Thickness. *Macromolecules* **2018,**

10. Albrecht, T.; Strobl, G., Temperature-Dependent Crystalline-Amorphous Structures in Linear Polyethylene: Surface Melting and the Thickness of the Amorphous Layers. *Macromolecules* **1995**

11. Jones, R. A. L., *Soft Condensed Matter*. Oxford University Press: Oxford, **2002**.

12. Zhang, M. C.; Guo, B.-H.; Xu, J., A Review on Polymer Crystallization Theories. *Crystals* **2017**

13. Albertsson, A.-C., *Long-Term Properties of Polyolefins*. **2004**.

14. Pantani, R.; Sorrentino, A.; Speranza, V.; Titomanlio, G., Molecular orientation in injection molding: Experiments and analysis. *Rheologica Acta* **2004**

15. Leary, M. A volume in Additive Manufacturing Materials and Technologies In *Design for Additive Manufacturing*, Leary, M., Ed. Elsevier: **2020**

16. Schultz, S. S. K. a. J. M., The Microstructure of Injection-Molded Semicrystalline Polymers: A Review. *POLYMER ENGINEERING AND SCIENCE* **1982**.

17. SWAN, P. R., Polyethylene -Unit Cell Variations with Temperature. *JOURNAL OF POLYMER SCIENCE* **1962**

18. Miao, M.; Zhang, M. L.; Doren, V.; Van Alsenoy, C.; Martins, J., Density functional calculations on the structure of crystalline polyethylene under high pressures. *The Journal of Chemical Physics* **2001**

19. Padden, F. J.; Keith, H. D., Spherulitic Crystallization in Polypropylene. *Journal of Applied Physics* **1959**

20. Butler, M. F.; Donald, A. M., A Real-Time Simultaneous Small- and Wide-Angle X-ray Scattering Study of in Situ Polyethylene Deformation at Elevated Temperatures. *Macromolecules* **1998**

21. Hobbs, J. K.; Miles, M. J., Direct Observation of Polyethylene Shish-Kebab Crystallization Using in-Situ Atomic Force Microscopy. *Macromolecules* **2001**

22. Keller, A.; Machin, M. J., Oriented crystallization in polymers. *Journal of Macromolecular Science, Part B* **1967**

23. Regrain, C.; Laiarinandrasana, L.; Toillon, S.; Saï, K., Multi-mechanism models for semi-crystalline polymer: Constitutive relations and finite element implementation. *International Journal of Plasticity* **2009**

24. Liu, Z.; Liu, X.; Li, L.; Zheng, G.; Liu, C.; Qin, Q.; Mi, L., Crystalline structure and remarkably enhanced tensile property of β-isotactic polypropylene via overflow microinjection molding. *Polymer Testing* **2019**

25. Dashan Mi, M. Z., Jie Zhang, Quantification of shish–kebab and b-crystal on the mechanicalproperties of polypropylene. *Journal of Applied Polymer Science* **2017**.

26. Schrauwen, B. A. G.; Breemen, L. C. A. v.; Spoelstra, A. B.; Govaert, L. E.; Peters, G. W. M.; Meijer, H. E. H., Structure, Deformation, and Failure of Flow-Oriented Semicrystalline Polymers. *Macromolecules* **2004**

27. Schrauwen, B. A. G.; Janssen, R. P. M.; Govaert, L. E.; Meijer, H. E. H., Intrinsic Deformation Behavior of Semicrystalline Polymers. *Macromolecules* **2004**

28. Somani, R. H.; Yang, L.; Zhu, L.; Hsiao, B. S., Flow-induced shish-kebab precursor structures in entangled polymer melts. *Polymer* **2005**

29. Tong, Y.; Lin, Y.; Wang, S.; Song, M., A study of crystallisation of poly (ethylene oxide) and polypropylene on graphene surface. *Polymer* **2015**

30. Ejikeme, P., Investigation of The Physicochemical Properties of Microcrystalline Cellulose From Agricultural Wastes I: Orange Mesocarp. *Cellulose* **2008**

31. Mohamad Haafiz, M. K.; Eichhorn, S. J.; Hassan, A.; Jawaid, M., Isolation and characterization of microcrystalline cellulose from oil palm biomass residue. *Carbohydrate Polymers* **2013**

32. Penttilä, P. Structural characterization of cellulosic materials using x-ray and neutron scattering. **2013**

33. Fengel, D.; Wegener, G., *Wood*. De Gruyter: **1983**

34. Huber, T.; Müssig, J.; Curnow, O.; Pang, S.; Bickerton, S.; Staiger, M. P., A critical review of all-cellulose composites. *Journal of Materials Science* **2012**

35. Müssig, J., Industrial Applications of Natural Fibres: Structure, Properties and Technical Applications. **2010**

36. Saito, T.; Kuramae, R.; Wohlert, J.; Berglund, L. A.; Isogai, A., An Ultrastrong Nanofibrillar Biomaterial: The Strength of Single Cellulose Nanofibrils Revealed via Sonication-Induced Fragmentation. *Biomacromolecules* **2013**

37. Larsson, P.; Berglund, L.; Wågberg, L., Highly ductile fibres and sheets by core-shell structuring of the cellulose nanofibrils. *Cellulose* **2014**

38. Fu, H.; Xu, H.; Liu, Y.; Yang, Z.; Kormakov, S.; Wu, D.; Sun, J., Overview of Injection Molding Technology for Processing Polymers and Their Composites. *ES Materials & Manufacturing* **2020**

39. Dakshinamoorthi, M.; Ghazaly, N.; R, V., Minimization of sink mark defects in injection molding process – Taguchi approach. *International Journal of Engineering, Science and Technology* **2010**

40. Angelloz, C.; Fulchiron, R.; Douillard, A.; Chabert, B.; Fillit, R.; Vautrin, A.; David, L., Crystallization of Isotactic Polypropylene under High Pressure (γ Phase). *Macromolecules* **2000**

41. Pantani, R.; Coccorullo, I.; Speranza, V.; Titomanlio, G., Morphology evolution during injection molding: Effect of packing pressure. *Polymer* **2007**

42. Wang, J.; Wang, L.; Bian, N.; Wang, D.; Wang, Y.; Zhang, Y.; Li, Q.; Shen, C., Influence of shear history on morphology, microstructure and mechanical properties of micro injection molded parts. *Huagong Xuebao/CIESC Journal* **2015**

43. Boyer, S. A. E.; Haudin, J.-M., Crystallization of polymers at constant and high cooling rates: A new hot-stage microscopy set-up. *Polymer Testing* **2010**

44. Wingstrand, S. L.; van Drongelen, M.; Mortensen, K.; Graham, R. S.; Huang, Q.; Hassager, O., Influence of Extensional Stress Overshoot on Crystallization of LDPE. *Macromolecules* **2017**

45. Zhou, H., *Computer modeling for injection molding : simulation, optimization, and control*. Wiley: New Jersey, **2013**

46. Fernandes, C.; Pontes, A.; Viana, J.; Gaspar-Cunha, A., Modeling and Optimization of the Injection-Molding Process: A Review. *Advances in Polymer Technology* **2016**

47. Larsson, P.; Wågberg, L., Towards natural-fibre-based thermoplastic films produced by conventional papermaking. *Green Chemistry* **2016**

48. Willmott, P., *An introduction to Synchrotron Radiation: Techniques and Applications*. John Wiley & Sons: **2011**

49. J.M.G Cowie, V. A., *Polymer Chemistry and Physics of Modern Materials Third Edition*. CRC Press: **2014**

50. Virtanen, T.; Penttilä, P. A.; Maloney, T. C.; Grönqvist, S.; Kamppuri, T.; Vehviläinen, M.; Serimaa, R.; Maunu, S. L., Impact of mechanical and enzymatic pretreatments on softwood pulp fiber wall structure studied with NMR spectroscopy and X-ray scattering. *Cellulose* **2015,**

51. Schmacke, S. Investigations of Polyethylene Materials by Means of X-ray Diffraction Artificial Ageing of Polyethylene Gas Pipes. der Technischen Universität Dortmund, **2010**

52. Möller, K. M. a. M., *Polymer Science: A Comprehensive Reference*. **2012**

53. O Bunk, M. B., T H Jensen, R Feidenhans'l, T Binderup, A Menzel and F Pfeiffer, Multimodal x-ray scatter imaging. *New Journal of Physics* **2009**

54. Henrich, B.; Bergamaschi, A.; Broennimann, C.; Dinapoli, R.; Eikenberry, E. F.; Johnson, I.; Kobas, M.; Kraft, P.; Mozzanica, A.; Schmitt, B., PILATUS: A single photon counting pixel detector for X-ray applications. *Nuclear Instruments and Methods in Physics Research Section A: Accelerators, Spectrometers, Detectors and Associated Equipment* **2009**

55. O'Connor, D. G.; Findley, W. N., Influence of normal stress on creep in tension and compression of polyethylene and rigid polyvinyl chloride copolymer. *Polymer Engineering and Science* **1962**

56. Sauer, J. A.; Mears, D.; Pae, K. D., Effects of hydrostatic pressure on the mechanical behaviour of polytetrafluoroethylene and polycarbonate. *European Polymer Journal - EUR POLYM J* **1970**

57. Colak, O.; Düşünceli, N., Modeling Viscoelastic and Viscoplastic Behavior of High Density Polyethylene (HDPE). *Journal of Engineering Materials and Technology-transactions of The Asme - J ENG MATER TECHNOL* **2006**

58. Pawlak, A.; Galeski, A., Plastic Deformation of Crystalline Polymers: The Role of Cavitation and Crystal Plasticity. *Macromolecules* **2005**

59. Clausen, A. H.; Polanco-Loria, M. A.; Berstad, T.; Hopperstad, S. Constitutive model for thermoplastics with structural applications. *International Journal of Impact Engineering,* **2010**

60. Arieby, R.; Mrabet, K.; Terfas, O.; Laurent, C.; Rahouadj, R., Anisotropic mechanical behavior of semi-crystalline polymers: Characterization and modeling of non-monotonic loading including damage. *Journal of Applied Polymer Science* **2016**

61. Martin Kroon, E. A., Elin Persson Jutemar, ; Viktor Petersson, L. P., Michael Dorn, Par Olsson Anisotropic Elastic-Viscoplastic Properties at Finite Strains of Injection-Moulded Low-Density Polyethylene. *Experimental Mechanics* **2017**

62. Takeshi Okano, A. K., Structural variation of native cellulose related to its source. *Biopolymers* **1986**

63. Büyüksarı, Ü.; As, N.; Dündar, T., Mechanical Properties of Earlywood and Latewood Sections of Scots Pine Wood. *Bioresources* **2017**

64. Wang, D.; Fu, F.; Lin, L., Molecular-level characterization of changes in the mechanical properties of wood in response to thermal treatment. *Cellulose* **2022**

65. Zhou, L.; Ke, K.; Yang, M.-B.; Yang, W., Recent progress on chemical modification of cellulose for high mechanical-performance Poly(lactic acid)/Cellulose composite: A review. *Composites Communications* **2021**

66. Haward, S. J.; Toda-Peters, K.; Shen, A. Q., Steady viscoelastic flow around high-aspect-ratio, low-blockage-ratio microfluidic cylinders. *Journal of Non-Newtonian Fluid Mechanics* **2018**

67. Li, D.; Zhou, L.; Wang, X.; He, L.; Yang, X., Effect of Crystallinity of Polyethylene with Different Densities on Breakdown Strength and Conductance Property. *Materials (Basel)* **2019**

68. Fernandes, A. N.; Thomas, L. H.; Altaner, C. M.; Callow, P.; Forsyth, V. T.; Apperley, D. C.; Kennedy, C. J.; Jarvis, M. C., Nanostructure of cellulose microfibrils in spruce wood. *Proceedings of the National Academy of Sciences* **2011**

69. Jakob, H. F.; Fengel, D.; Tschegg, S. E.; Fratzl, P., The Elementary Cellulose Fibril in Picea abies: Comparison of Transmission Electron Microscopy, Small-Angle X-ray Scattering, and Wide-Angle X-ray Scattering Results. *Macromolecules* **1995**

70. O'Sullivan, A. C., Cellulose: the structure slowly unravels. *Cellulose* **1997**

71. Keller, A.; O'Connor, A., Large Periods in Polyethylene: the Origin of Low-Angle X-ray Scattering. *Nature* **1957**

72. Leung, W. M., Studies of low molecular weight polyethylene single crystals by differential scanning calorimetry. *Colloid and Polymer Science* **1985**

73. van Drongelen, M.; Cavallo, D.; Balzano, L.; Portale, G.; Vittorias, I.; Bras, W.; Alfonso, G. C.; Peters, G., Structure Development of Low-Density Polyethylenes During Film Blowing: A Real-Time Wide-Angle X-ray Diffraction Study. *Macromolecular Materials and Engineering* **2014**

74. Guo, H.; Rinaldi, R. G.; Broudin, M.; Tayakout, S.; Lame, O., Anisotropic deformation and failure behaviors of the necked HDPE materials induced by oligo-cyclic loading. *Polymer* **2021**

75. Jiang, J.; Liu, X.; Lian, M.; Pan, Y.; Chen, Q.; Liu, H.; Zheng, G.; Guo, Z.; Schubert, D. W.; Shen, C.; Liu, C., Self-reinforcing and toughening isotactic polypropylene via melt sequential injection molding. *Polymer Testing* **2018**

76. Zhou, M.; Li, X.-p.; Jin, M.; Xia, C.; Shen, K.-z.; Zhang, J., Simultaneously improving the tensile and impact properties of isotactic polypropylene with the cooperation of co-PP and β-nucleating agent through pressure vibration injection molding. *Chinese Journal of Polymer Science* **2016**

77. Lin, L.; Argon, A., Review Structure and plastic deformation of polyethylene. *Journal of Materials Science* **1994**

78. Bowden, P. B.; Young, R. J., Deformation mechanisms in crystalline polymers. *Journal of Materials Science* **1974**

79. Kennedy, C.; Šturcová, A.; Jarvis, M.; Wess, T., Hydration effects on spacing of primary-wall cellulose microfibrils: A small angle X-ray scattering study. *Cellulose* **2007**

80. Hitchcock, A.; Morin, C.; Zhang, X.; Araki, T.; Dynes, J.; Stöver, H.; Brash, J.; Lawrence, J.; Leppard, G., Soft X-ray spectromicroscopy of biological and synthetic polymer systems. *Journal of Electron Spectroscopy and Related Phenomena* **2005**

81. Paris, O.; Li, C.; Siegel, S. D.; Weseloh, G.; Emmerling, F.; Riesemeier, H.; Erko, A. I.; Fratzl, P., A new experimental station for simultaneous X-ray microbeam scanning for small- and wide-angle scattering and fluorescence at BESSY II. *Journal of Applied Crystallography* **2006**

82. Pirkkalainen, K.; Peura, M.; Leppänen, K.; Salmi, A.; Meriläinen, A.; Saranpaa, P.; Serimaa, R., Simultaneous X-ray diffraction and X-ray fluorescence microanalysis on secondary xylem of Norway spruce. *Wood Science and Technology* **2011**